energy&fuels

Article

Cite This: Energy Fuels 2018, 32, 6090−6097

pubs.acs.org/EF

Adsorptive Separation of CO_2 from Multicomponent Mixtures of Flue Gas in Carbon Nanotube Arrays: A Grand Canonical Monte Carlo Study

Sauradeep Majumdar, Manish Maurya, and Jayant K. Singh*

Department of Chemical Engineering, Indian Institute of Technology Kanpur, Kanpur 208016, India

Supporting Information

ABSTRACT: Grand canonical Monte Carlo (GCMC) simulations have been performed to investigate the adsorption and separation behavior of ternary and quaternary gaseous mixtures of CO_2, along with H_2S, SO_2, and N_2, in bundles of aligned double-walled carbon nanotubes with a diameter of 3 nm and an intertube distance of 0.5 nm. All of the simulations are performed at 303 K and at pressures varying between 0 and 3 bar. The GCMC results are then compared to the ideal adsorbed solution theory (IAST) predictions. For the ternary mixture $H_2S-CO_2-N_2$, the results show that CO_2 has the highest adsorption among the three components. The IAST predictions agree reasonably well with the GCMC data for the ternary mixture, except for H_2S. For the quaternary mixture $H_2S-SO_2-CO_2-N_2$, it is observed that initially CO_2 has the highest adsorption up until around 2 bar, whereafter there is a crossover by SO_2 to have the highest adsorption. IAST fails to predict the adsorption behavior of the quaternary mixture involving SO_2.

INTRODUCTION

The increasing amount of atmospheric carbon dioxide (CO_2), a major component of the flue gas emitted from fossil-fuel-burning power plants, is considered to be one of the primary factors leading to global warming and climate change.[1−4] Among different techniques, adsorptive separation of CO_2 has been recognized as an efficient post-combustion capture technique to stabilize the atmospheric content of CO_2.[5−9] In reality, what we deal with are not pure gases but mixtures of different gases. In this context, it is therefore important to understand how the adsorption of CO_2 would be affected when it is present with the other components of flue gas. In the actual flue gas emitted from power plants, along with CO_2, there would be gases such as N_2, SO_2, H_2S, etc. Incidentally, some of these gases themselves pose major threats to the environment. Sulfur dioxide (SO_2), for example, is a major air pollutant. SO_2 emissions are known to cause acid rain, which has a detrimental effect on soil fertility as well as the walls of buildings and monuments.[10,11] Hydrogen sulfide (H_2S) emissions have been reported to be toxic for the human body and corrosive for machines.[12]

There have been several studies on the adsorption of CO_2 on different adsorbents, such as carbon nanotubes (CNTs),[13−15] activated carbons,[16−18] zeolites,[19,20] and metal−organic frameworks (MOFs).[21−23] Although some MOFs and zeolites are reported to have higher adsorption capacities as a result of their high micropore volume, they are not much stable under humid conditions.[11] Carbonaceous materials are more attractive in this respect. Among carbonaceous materials, activated carbons and CNTs have been the most widely studied adsorbents. Activated carbons, however, possess a disadvantage in the fact that they do not exhibit a particularly strong selectivity toward CO_2.[24] As a result, they are not very effective in the post-combustion carbon capture process.

On the other hand, CNTs have been widely studied in the past decade as adsorbents of CO_2, SO_2, H_2, and N_2,[25−27] mainly as a result of their desirable properties, such as hollow cylindrical geometry, low mass density, and large specific area.[28,29] Purified single-walled carbon nanotubes (SWCNTs) have been shown to adsorb almost twice the volume of CO_2 compared to activated carbon.[30] Liu et al.[31] studied the separation of CO_2 from natural gas in CNTs and disordered carbon materials, such as silicon-carbide-derived carbon (SiC-DC), and found CNTs to be the better performers. There have been some adsorption studies with a new class of porous materials called carbon material of Korea (CMK), but their CO_2 adsorption capacties are not very high, ≈0.8 mmol/g at 1 bar and 303 K,[32] compared to ≈5 mmol/g for double-walled carbon nanotube (DWCNT) bundles at the same conditions.[33] Wang et al. studied the adsorption of binary mixtures of H_2S and SO_2 with CH_4, SO_2, and N_2 in bundles of SWCNTs, thus providing useful information about sulfur gas capture.[27] Rahimi et al.[34] studied the adsorption and separation of binary and ternary mixtures of CO_2, SO_2, and N_2 in bundles of DWCNTs. However, not much was studied about ternary mixtures in detail. The selectivity results from their studies indicate that DWCNTs are excellent materials for gas purification. They also looked into the effect of adding charge to SWCNTs on the adsorption of CO_2.[15] The adsorption increased significantly when the CNTs had a positive charge, while a negative charge caused the adsorption to decrease compared to neutral CNT arrays. It is to be noted that, in comparison to SWCNTs, which are expensive and more difficult to synthesize,[35] closed pack bundles of DWCNTs are easy to obtain[36] and, thus, provide an advantage from an application point of view.

Among all of the adsorption and separation studies, there are few that have investigated in detail the behavior of ternary and higher mixtures of flue gas components. Biase et al.[24] studied

Received: February 23, 2018
Revised: April 11, 2018
Published: April 16, 2018

DOI: 10.1021/acs.energyfuels.8b00649
Energy Fuels 2018, 32, 6090−6097

the adsorption and separation of ternary and quaternary mixtures of CO_2−N_2−O_2−H_2O on activated carbon. However, to the best of our knowledge, there has not been any detailed study on the adsorption and separation of ternary and quaternary gaseous mixtures of H_2S, SO_2, CO_2, and N_2 on DWCNTs.

In view of the above, we therefore try to investigate the adsorption of ternary (H_2S−CO_2−N_2) and quaternary (H_2S−SO_2−CO_2−N_2) mixtures of flue gas components in bundles of aligned DWCNTs using the grand canonical Monte Carlo (GCMC) method. Apart from obtaining realistic estimates of the adsorption of CO_2, this work thus also addresses the control of emissions of other environmentally harmful gases, such as SO_2 and H_2S. The effect of the tube diameter and intertube distance having already been exhaustively studied,[34,37,38] we use the optimum values reported for single gas adsorption. We then compare the results of GCMC simulations to those obtained from the ideal adsorbed solution theory[39] (IAST) predictions.

MODELS AND METHODS

Potential Models. The interaction energy between two molecules is expressed as the sum of Lennard−Jones (LJ) and Coulombic interactions as given below

$$E = \sum_{i,j} 4\varepsilon_{ij}\left[\left(\frac{\sigma_{ij}}{r_{ij}}\right)^{12} - \left(\frac{\sigma_{ij}}{r_{ij}}\right)^{6}\right] + \sum_{i,j}\frac{Cq_iq_j}{\varepsilon r_{ij}} \quad (1)$$

where the first term on the right-hand side represents the standard 12-6 Lennard−Jones (LJ) potential and the second term represents the Coulombic pairwise interactions between sites i and j of two molecules.

We consider the DWCNTs as rigid structures and describe them using the LJ potential of the AMBER96 force field,[40] which has been used in work of a similar type.[38,41] The transferable potentials for phase equilibria (TraPPE) model proposed by Potoff et al.[42] is used to describe CO_2 and N_2. For SO_2 and H_2S, we use the model developed by Ketko et al.[43] and Nath et al.,[44] respectively. All of the energy parameters are listed in Table 1.

Table 1. Interaction Parameters of Adsorbates and DWCNT Adsorbent

species	site	ε (kcal/mol)	σ (Å)	q (e)
CO_2	C	2.8	0.054	0.7
	O	3.05	0.157	−0.35
N (in N_2)	N	3.31	0.072	−0.482
COM (in N_2)	N	0.0	0.0	0.964
SO_2	S	3.39	0.147	0.59
	O	3.05	0.157	−0.295
H_2S	H	0.98	0.008	0.124
	S	3.72	0.497	−0.248
DWCNT	C	3.4	0.086	0.0

Simulation Details. On the basis of the experimentally observed structure of Rahimi et al.,[14] the DWCNT bundles are arranged on a hexagonal lattice and periodic boundary conditions are used in all three directions. The simulated system size is large enough to avoid a system size effect on the statistics of reported adsorption data. The diameter of the bundles and the intertube distance are taken to be 3 and 0.5 nm, respectively, the optimum values reported for single-gas adsorption.[34] The simulation box length in the direction of the CNT axes, L_z, is equal to the CNT length, which is 7.614 nm. It is to be noted here that adsorption isotherms have been found to be insensitive to the CNT length.[38] The simulation box lengths in the other two directions, L_x and L_y, are taken to be 4.361 and 7.554 nm, respectively.

The GCMC method is used to calculate the adsorption and separation coefficients of gases. We kept the temperature fixed at 303 K. Three Monte Carlo moves, displacement, addition/removal, and rotation, are employed with the respective probabilities being 0.2, 0.7, and 0.1. To generate the adsorption isotherms, the simulations are conducted at different chemical potentials to span the region between 0 and 3 bar. To account for the non-ideality of the gases, the excess chemical potentials of the individual components in the gas mixture are calculated using Widom's test particle insertion method.[45] The simulations consist of equilibration and production runs of 1.5×10^7 Monte Carlo steps each. A cutoff distance of 1.5 nm is used for both Coulombic and LJ interactions. The LJ interactions between dissimilar atoms are approximated using Lorentz−Berthelot rules.[46] Ewald summations are used to correct the long-range electrostatic interactions. All of the simulations in this work have been performed using an in-house Monte Carlo code written in C++, validated by matching fluid properties with the National Institute of Standards and Technology (NIST).[47] The code has also been used to study gas adsorption in porous materials.[11,32]

The composition of the flue gases strongly depends upon its type. In this study, the compositions taken are based on coal-fired flue gases.[48] For the ternary mixture of H_2S−CO_2−N_2, we have used the molar ratio of 1:19:80, and for the quaternary mixture of H_2S−SO_2−CO_2−N_2, the molar ratio taken is 0.5:1.5:18.5:79.5.

Adsorption Theory. In GCMC simulations, we obtain the absolute number of adsorbed particles (N_{ad}) in the simulation box. However, data from experiments are generally reported in terms of excess adsorption (N_{excess}). The absolute adsorption is thus converted into excess adsorption using the following relation:

$$N_{excess} = N_{ad} - \rho_b V_{free} \quad (2)$$

where ρ_b is the bulk density of the adsorbate, obtained from independent GCMC simulations at the same thermodynamic conditions, and V_{free} is the accessible volume for the fluid molecules, which can be calculated by different methods.[49−51] In this work, the helium adsorption technique, as described by Myers et al., is used to calculate the free volume and is explained below briefly.[51]

In the low-pressure limit, the excess adsorption is given by

$$N_{excess} = \frac{BP}{RT} \quad (3)$$

where B is the adsorption second virial coefficient or Henry's law coefficient. For porous adsorbents, B is expressed as

$$B = \frac{1}{m}\int e^{-E(r)/kT}\,dr - V_{free} \quad (4)$$

where E is the gas−solid potential energy of a single molecule and m is the mass of a representative sample of solid adsorbent used for integration. The integration performed over the sample vanishes inside the solid, where $E \to \infty$. For the theory to mimic the experiment, N_{excess} and B for helium must be 0, which implies that

$$V_{free} = \frac{1}{m}\int e^{-E(r)/kT}\,dr \quad \text{(for He)} \quad (5)$$

The accessible volume is thus obtained from the above expression.

The adsorption selectivity in a binary mixture of components i and j is calculated as

$$S_{i/j} = \frac{x_i}{y_i}\Big/\frac{x_j}{y_j} \quad (6)$$

where x_i and y_i are the mole fractions of component i in the adsorbed and bulk phases, respectively.

IAST. The IAST is used to predict the adsorption behavior of multicomponent mixtures from single-component isotherms.[39] It is one of the most widely used models for this purpose, especially in the low-pressure region. We have described below the basic equations of IAST.

For each component of a mixture, the following equation holds based on an analogy with Raoult's law:

$$Py_i = x_iP_i(\pi) \quad (7)$$

where P is the total pressure in the bulk gas phase, P_i is the bulk pressure of component i that corresponds to the spreading pressure

DOI: 10.1021/acs.energyfuels.8b00649
Energy Fuels 2018, 32, 6090−6097

π of the mixture, and x_i and y_i are as explained above in eq 6. The molar fractions of the adsorbed species sum to 1, implying

$$\sum_{i=1}^{N} \frac{Py_i}{P_i} = 1 \tag{8}$$

where N is the number of components in the mixture. For each component, P_i and π are related through

$$\frac{\pi A}{RT} = \int_0^{P_i} \frac{n_i(P)}{P}\, dP \tag{9}$$

where A is the surface area of the adsorbent, R is the universal gas constant, T is the temperature, and $n_i(P)$ is the amount adsorbed at pressure P. Three different models, namely, Langmuir, Freundlich, and dual-site Langmuir, were used to fit the single-component isotherms, and they are shown in the Supporting Information. The Langmuir model is found to provide the best fit among the three, as indicated by the lowest sum of squared error (SSE) values.

It is important to note here that, for binary mixtures, Levan and Vermeulen presented an important solution of eqs 7−9 that could be used directly to obtain the adsorbed amount of each species.[52] However, for ternary and higher mixtures, the solution becomes tricky and eqs 7−9 along with the fitted parameters of the Langmuir model (Table S1 of the Supporting Information) are used to calculate the adsorption of component i, n_i, in the ternary and quaternary mixtures, following the method as described by Do.[53]

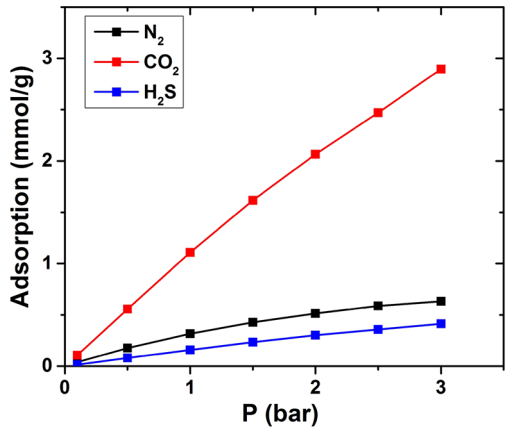

Figure 1. Excess adsorption isotherms of H_2S, CO_2, and N_2 in a H_2S−CO_2−N_2 ternary mixture system on DWCNT arrays with an inner tube diameter of 3 nm and an intertube distance of 0.5 nm at T = 303 K. P refers to the total pressure of the mixture. Error bars are smaller than the symbols.

RESULTS AND DISCUSSION

Ternary Mixture. Figure 1 shows the excess adsorption isotherms of a ternary mixture of H_2S−CO_2−N_2 at a molar ratio of 1:19:80 on a bundle of 3 nm diameter DWCNTs as a function of the total bulk pressure. As expected, the excess adsorption increases with an increase in the pressure for all of the components in the mixture, however with individual variations. CO_2 shows the highest adsorption among the three, although, in the bulk, there is more N_2 than the other two. At 1 bar and 303 K, the adsorption amount of CO_2 turns out to be 1.11 mmol/g. Interesting to note here is that, when the bulk gas consists of pure CO_2, then the adsorption amount of CO_2 is reported to be ≈5 mmol/g.[33] Thus, a drastic decline is observed in the CO_2 adsorption amount when present in a mixture along with other gases. N_2, as a result of its inert nature, has a very weak interaction with CNT, and thus, despite occupying almost 80% of the bulk volume, its adsorption amount is quite less compared to CO_2. Although H_2S has a higher selectivity with respect to both CO_2 and N_2 (Figure 3), it has the least adsorption amount among the three as a result of its lowest bulk composition.

Figure 2 shows snapshots of adsorption of a H_2S−CO_2−N_2 ternary mixture system on arrays of DWCNTs at three different pressures: 1, 2, and 3 bar. At low pressures of around 1 bar, the inner and groove regions start filling up first. The interstitial region starts filling up at higher pressures of around 3 bar when the inner and groove regions are almost saturated. Previously, Agnihotri et al.[54] and Bienfait et al.[55] also found out that grooves are the most favorable sites for adsorption on CNT arrays. The rapid increase in the adsorption amount of CO_2 (cyan and red) with increasing pressure can be observed from the snapshots. N_2 (blue) and H_2S (white and yellow) have relatively low adsorption amounts, with H_2S having the least.

From the selectivity curves (Figure 3), we observe that the selectivity of CO_2 over N_2 increases steadily over the entire pressure range. N_2, being inert, has a very weak interaction with the DWCNTs compared to CO_2. The selectivity values, ranging

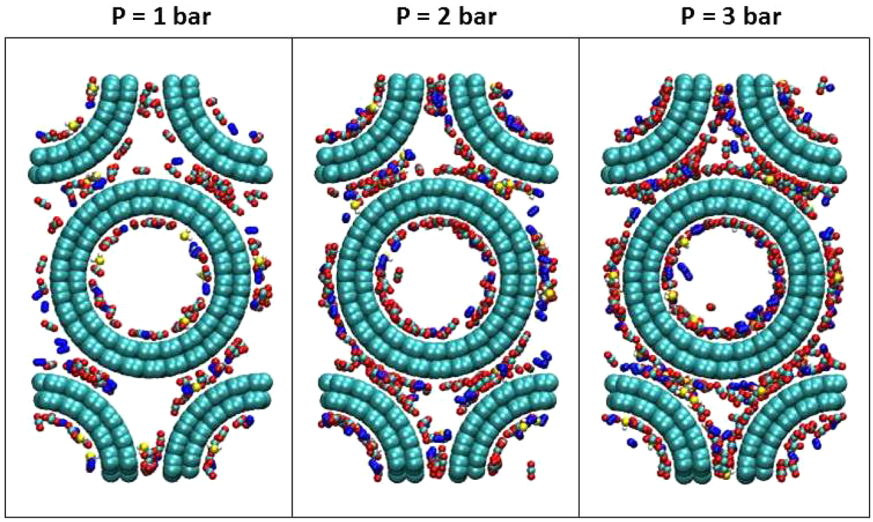

Figure 2. Snapshots of adsorption of a H_2S−CO_2−N_2 ternary mixture system on DWCNT arrays with an inner tube diameter of 3 nm and an intertube distance of 0.5 nm at T = 303 K. P refers to the total pressure of the mixture, with (cyan and red) CO_2, (blue) N_2, and (white and yellow) H_2S.

DOI: 10.1021/acs.energyfuels.8b00649
Energy Fuels 2018, 32, 6090−6097

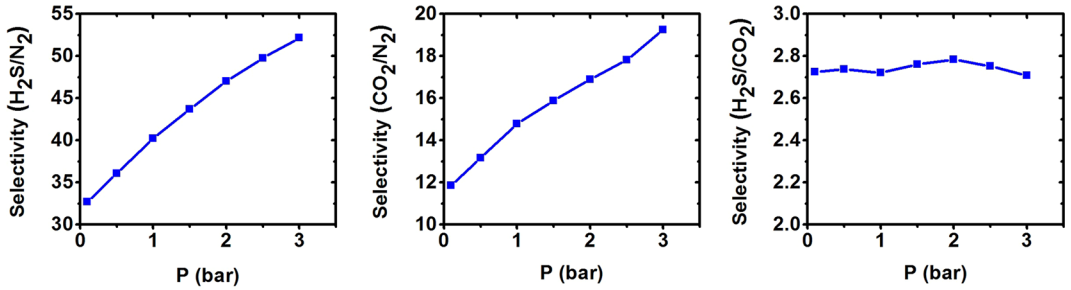

Figure 3. Selectivities, as computed by GCMC, in a $H_2S-CO_2-N_2$ ternary mixture system on DWCNT arrays with an inner tube diameter of 3 nm and an intertube distance of 0.5 nm at T = 303 K. P refers to the total pressure of the mixture. Error bars are smaller than the symbols.

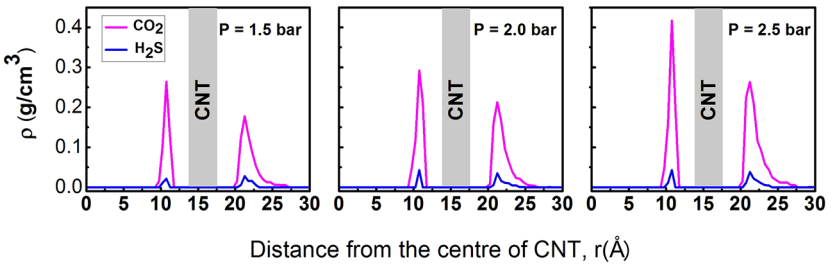

Figure 4. Density profiles for CO_2 (magenta) and H_2S (blue) adsorption in a $H_2S-CO_2-N_2$ ternary mixture system on DWCNT arrays with an inner tube diameter of 3 nm and an intertube distance of 0.5 nm at T = 303 K. P refers to the total pressure of the mixture.

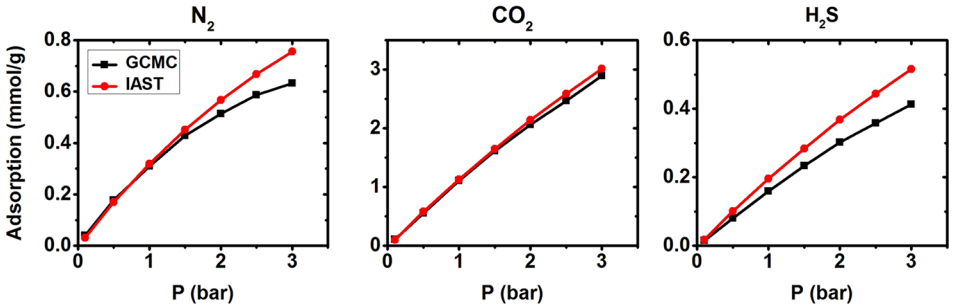

Figure 5. Comparison of excess adsorption data from IAST and GCMC simulations of a $H_2S-CO_2-N_2$ ternary mixture system on DWCNT arrays with an inner tube diameter of 3 nm and an intertube distance of 0.5 nm at T = 303 K. P refers to the total pressure of the mixture. Error bars are smaller than the symbols.

between 12 and 20, are much higher than the observed values of Biase et al.,[24] which range approximately between 6 and 7. The selectivity of H_2S over N_2 also increases smoothly with the pressure, with the reason being that H_2S, being a highly polar molecule, exhibits a stronger interaction with the DWCNTs compared to N_2. The selectivity of H_2S over CO_2, however, follows a different trend. The selectivity of H_2S over CO_2 remains more or less constant around the 2.7 mark, followed by a slight decrease after 2 bar. Previously, Wang et al.[27] also found the selectivity of H_2S over CO_2, in a binary mixture, to be almost constant with pressure. From Figure 1, it is observed that the H_2S adsorption curve becomes almost saturated at around 2 bar, whereas the corresponding curve for CO_2 keeps on increasing steadily. Thus, after 2 bar, we observe the decrease in selectivity of H_2S over CO_2.

To confirm the reasoning, we also calculated the density profiles of H_2S and CO_2 at pressures around 2 bar, i.e., at 1.5, 2, and 2.5 bar (Figure 4). First, what we observe is that both the inner and outer adsorption of CO_2 increases from 1.5 to 2.5 bar, with the inner adsorption being higher in all of the cases. However, for H_2S, there is hardly any substantial change in the density profiles between 2 and 2.5 bar. This illustrates the fact that the H_2S excess adsorption isotherm becomes more or less saturated at around 2 bar. Thus, the selectivity of H_2S over CO_2 decreases after 2 bar.

Figure 5 shows the comparison of excess adsorption isotherms from GCMC simulations and IAST predictions. The IAST predictions agree reasonably well with the simulation data for N_2, with slight deviations at higher pressures. Thus, N_2 behaves more or less ideally in the adsorbed phase. Even for CO_2, it is observed that the IAST predictions are quite in line with the GCMC simulation data, thereby indicating that CO_2 too behaves ideally in the adsorbed phase. This, however, is not true for H_2S. For H_2S, except at low pressures, the IAST curve deviates from the GCMC curve, with the difference between them increasing with increasing pressure. Being a highly polar molecule, H_2S exhibits stronger interactions with the other two gases as well as with the CNT carbons. Its behavior in the adsorbed phase, therefore, deviates significantly from ideality.

Quaternary Mixture. Figure 6 shows the excess adsorption isotherms of a quaternary mixture of $H_2S-SO_2-CO_2-N_2$ at a molar ratio of 0.5:1.5:18.5:79.5 on a bundle of 3 nm diameter DWCNTs as a function of the total bulk pressure. The adsorption behaviors of N_2 and H_2S are found to be similar to that

DOI: 10.1021/acs.energyfuels.8b00649
Energy Fuels 2018, 32, 6090−6097

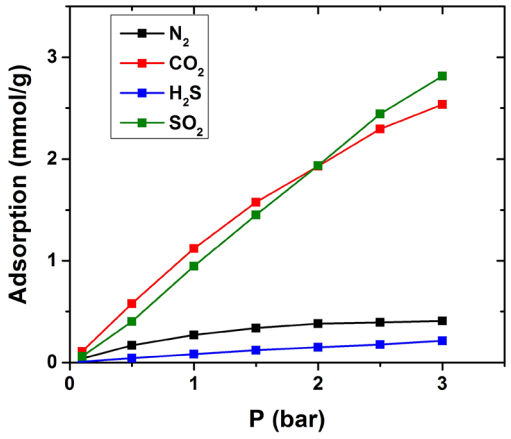

Figure 6. Excess adsorption isotherms of H_2S, SO_2, CO_2, and N_2 in a H_2–SO_2–CO_2–N_2 quaternary mixture system on DWCNT arrays with an inner tube diameter of 3 nm and an intertube distance of 0.5 nm at T = 303 K. P refers to the total pressure of the mixture. Error bars are smaller than the symbols.

obtained from the ternary isotherms. Interesting to note here is that CO_2 shows the highest adsorption among the four components up until around 2 bar, whereafter SO_2 crosses over CO_2 to have the highest adsorption. Now, as a result of its low bulk composition, SO_2 has a lower adsorption amount than CO_2 initially but with an increasing pressure, and as a result of its high selectivity over CO_2 (Figure 7), it manages to crossover the CO_2 curve at around 2 bar.

The selectivity of SO_2 over CO_2 increases steadily over the studied pressure range. SO_2 has a stronger interaction with CNT than CO_2as a result of it is highly polar nature. This contributes to the crossing over of CO_2 by SO_2 at around 2 bar in the excess adsorption isotherm. The selectivity of SO_2 over H_2S also exhibits a more or less steady increase over the studied pressure range. The selectivity of H_2S over CO_2 remains more or less constant up until around 2 bar, quite like the case of the ternary mixture. However, after 2 bar, instead of decreasing like in the case of the ternary mixture, the selectivity shows an increase. A probable reason for this could be that, unlike the ternary mixture, in the quaternary mixture, CO_2 faces stiff competition from SO_2 to become the highest adsorbate after 2 bar. Hence, the CO_2 adsorption amount after 2 bar does not increase as much as in the case of the ternary mixture. For instance, in the case of the ternary mixture, the CO_2 adsorption amount at 3 bar is 2.89 mmol/g, whereas for the quaternary mixture, it is 2.54 mmol/g.

Figure 8 shows snapshots of adsorption of a H_2S–SO_2–CO_2–N_2 quaternary mixture system on arrays of DWCNTs at three different pressures: 1, 2, and 3 bar. Quite like the ternary mixture, the inner and groove regions start becoming filled up at lower pressures. The gas molecules start adsorbing in the interstitial region once the inner and groove regions become saturated.

Figure 9 shows the density profiles of CO_2 and SO_2 at pressures around 2 bar: 1, 2, and 3 bar. At all three pressures, the

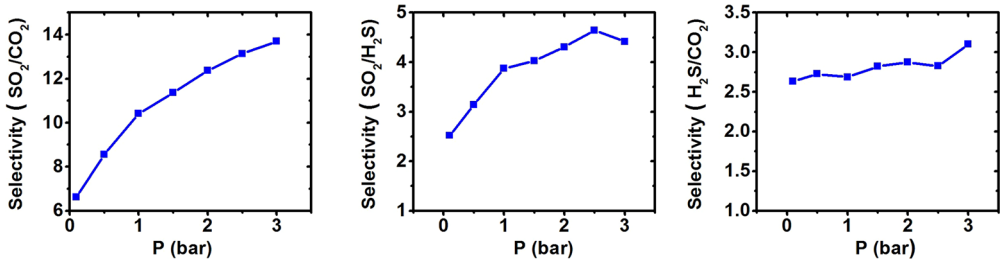

Figure 7. Selectivities as computed by GCMC in a H_2S–SO_2–CO_2–N_2 quaternary mixture system on DWCNT arrays with an inner tube diameter of 3 nm and an intertube distance of 0.5 nm at T = 303 K. P refers to the total pressure of the mixture. Error bars are smaller than the symbols.

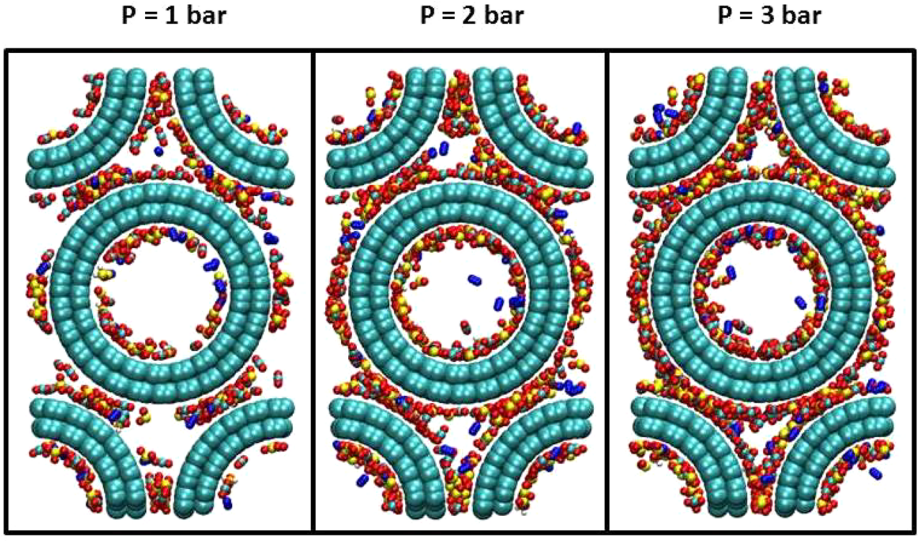

Figure 8. Snapshots of adsorption of a H_2S–SO_2–CO_2–N_2 quaternary mixture system on DWCNT arrays with an inner tube diameter of 3 nm and an intertube distance of 0.5 nm at T = 303 K. P refers to the total pressure of the mixture, with (cyan and red) CO_2, (blue) N_2, (white and yellow) H_2S, and (yellow and red) SO_2.

DOI: 10.1021/acs.energyfuels.8b00649
Energy Fuels 2018, 32, 6090–6097

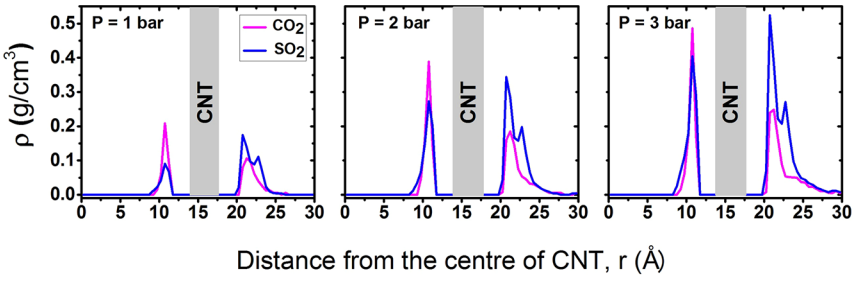

Figure 9. Density profiles for (magenta) CO_2 and (blue) SO_2 adsorption in a $H_2S-SO_2-CO_2-N_2$ quaternary mixture system on DWCNT arrays with an inner tube diameter of 3 nm and an intertube distance of 0.5 nm at T = 303 K. P refers to the total pressure of the mixture.

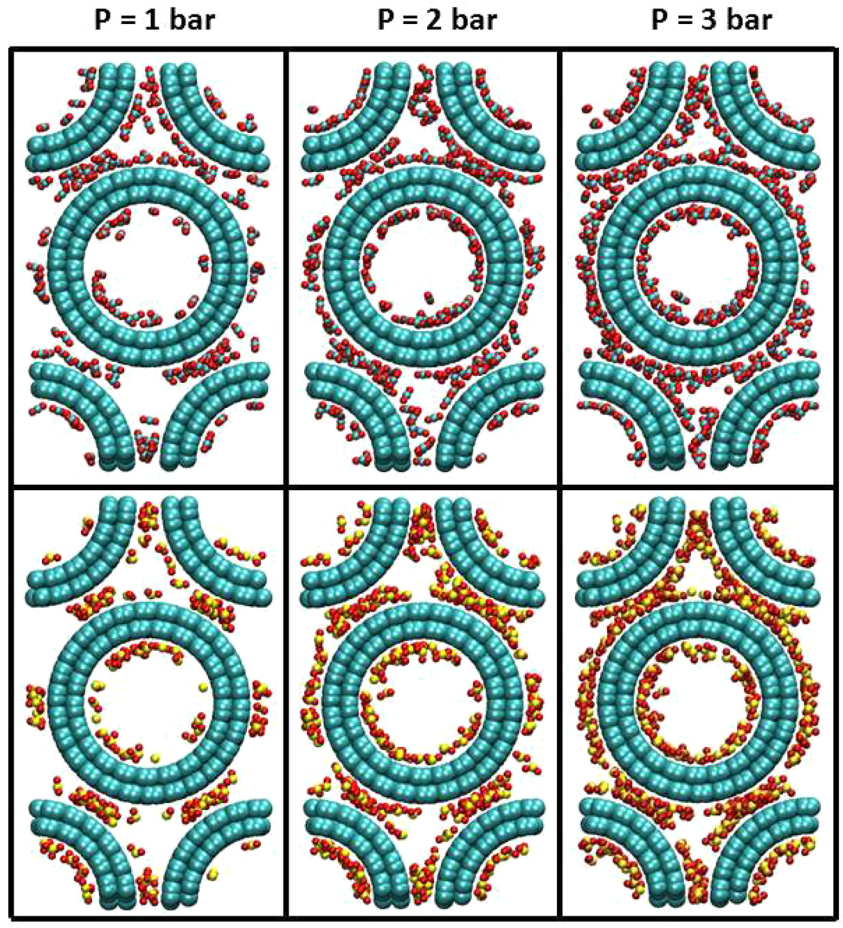

Figure 10. Snapshots of adsorption of (top) CO_2 and (bottom) SO_2 in a $H_2S-SO_2-CO_2-N_2$ quaternary mixture system on DWCNT arrays with an inner tube diameter of 3 nm and an intertube distance of 0.5 nm at T = 303 K. P refers to the total pressure of the mixture.

inner adsorption of SO_2 is less than that of CO_2. However, the outer adsorption of SO_2 is more than that of CO_2, and with increasing pressure, the rate of growth of the outer adsorption of SO_2 is higher than that of CO_2. Thus, beyond 2 bar, the total amount of SO_2 adsorbed, the sum of inner and outer, is more than that of CO_2, thereby confirming the crossover in the adsorption isotherm. This behavior can also be visualized from Figure 10. Because SO_2 has a higher affinity toward CNT than CO_2, it prefers to adsorb outside the CNT in the groove regions, where it finds more carbon atoms of the CNT. We thus observe the outer adsorption of SO_2 to be higher than that of CO_2.

Like in the case of the ternary mixture, we compared the GCMC simulation data to those obtained from the IAST predictions (Figure 11). However, the agreement is not as good as in the case of the ternary mixture, with the isotherms of SO_2 showing the highest deviation. This is due to the strongly interacting nature of SO_2. The presence of a highly polar molecule, such as SO_2, in the system leads to the high deviations from ideality, as seen in this quaternary mixture. Additionally, it is to be noted that ideal gases have no interactions with one another. Increasing the number of real components in the mixture increases the interactions between the components, thereby leading to non-ideal behavior. IAST can therefore not accurately predict the adsorption behavior of such systems.

CONCLUSION

In this work, we used GCMC simulations to study the adsorption behavior of CO_2 in bundles of aligned DWCNTs when present with other gases, H_2S, SO_2, and N_2, in ternary and quaternary

DOI: 10.1021/acs.energyfuels.8b00649
Energy Fuels 2018, 32, 6090−6097

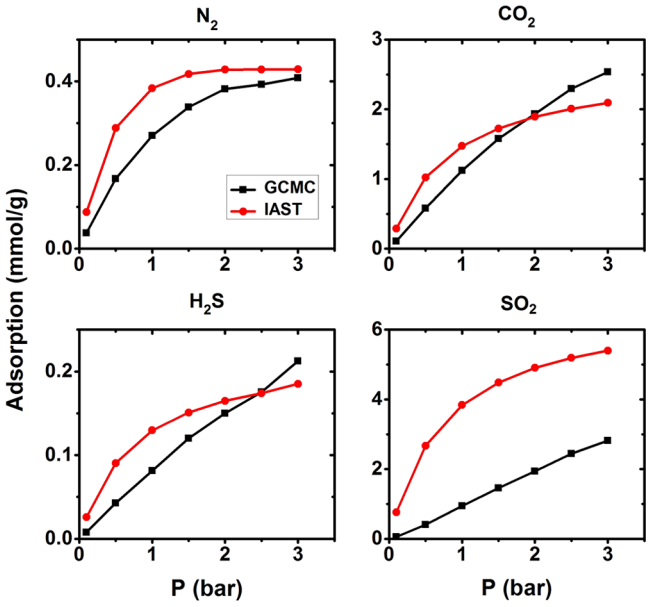

Figure 11. Comparison of excess adsorption data from IAST and GCMC simulations of a $H_2S–SO_2–CO_2–N_2$ quaternary mixture system on DWCNT arrays with an inner tube diameter of 3 nm and an intertube distance of 0.5 nm at T = 303 K. P refers to the total pressure of the mixture. Error bars are smaller than the symbols.

mixtures. At 1 bar and 303 K, the CO_2 adsorption amount is found to be 1.11 mmol/g. Thus, CO_2 adsorption does become affected when components such as SO_2 and H_2S are present in the mixture. We also obtain estimates of adsorption of the other gas components and the separation behavior of the mixtures.

For the ternary mixture, the simulation results show that CO_2 has the highest adsorption amount among the three components. The highest selectivity is observed between H_2S and N_2, followed by CO_2 and N_2 and finally H_2S and CO_2. In the case of the quaternary mixture, CO_2 shows the highest adsorption up until around 2 bar, whereafter SO_2 becomes the highest adsorbate. SO_2 is found to have a higher selectivity than CO_2 toward DWCNT, and from the high selectivity values obtained, we can thus confirm the excellent potential of this material for gas purification.

We then compared the GCMC results to the predictions obtained from IAST. The IAST predictions agree reasonably well with the GCMC simulation data for CO_2 and N_2 in the ternary mixture. For H_2S, we observe a deviation between the IAST and GCMC results, which increases with increasing pressure. For the quaternary mixtures, there is a significant deviation between the IAST and GCMC data, with the maximum deviation being for SO_2. IAST thus fails to predict the adsorption of mixtures involving strong interacting molecules, such as SO_2.

■ ASSOCIATED CONTENT

Supporting Information

The Supporting Information is available free of charge on the ACS Publications website at DOI: 10.1021/acs.energyfuels.8b00649.

Langmuir isotherm graphs (Figure S1) and parameters (Table S1) for pure component adsorption, Freundlich isotherm graphs (Figure S2) and parameters (Table S2) for pure component adsorption, and dual-site Langmuir isotherm graphs (Figure S3) and parameters (Table S3) for pure component adsorption (PDF)

■ AUTHOR INFORMATION

Corresponding Author

*Telephone: 0512-259-6141. Fax: 0512-259-0104. E-mail: jayantks@iitk.ac.in.

ORCID

Jayant K. Singh: 0000-0001-8056-2115

Notes

The authors declare no competing financial interest.

■ ACKNOWLEDGMENTS

The authors thank the Ministry of Earth Sciences, Government of India. The computational facility has been provided by High Performance Computing (HPC), Computer Center, Indian Institute of Technology Kanpur, India.

■ REFERENCES

(1) Younas, M.; Sohail, M.; Leong, L. K.; Bashir, M. J. K.; Sumathi, S. Feasibility of CO_2 adsorption by solid adsorbents: A review on low-temperature systems. *Int. J. Environ. Sci. Technol.* **2016**, *13*, 1839−1860.

(2) Mondal, M. K.; Balsora, H. K.; Varshney, P. Progress and trends in CO_2 capture/separation technologies: A review. *Energy* **2012**, *46*, 431−441.

(3) Jacobson, M. Z. Review of solutions to global warming, air pollution, and energy security. *Energy Environ. Sci.* **2009**, *2*, 148−173.

(4) Aaron, D.; Tsouris, C. Separation of CO_2 from Flue Gas: A Review. *Sep. Sci. Technol.* **2005**, *40*, 321−348.

(5) Grande, C. A.; Rodrigues, A. E. Electric Swing Adsorption for CO_2 removal from flue gases. *Int. J. Greenhouse Gas Control* **2008**, *2*, 194−202.

(6) Yu, C.-H.; Huang, C.-H.; Tan, C.-S. A Review of CO_2 Capture by Absorption and Adsorption. *Aerosol Air Qual. Res.* **2012**, *12*, 745−769.

(7) Lee, Z. H.; Lee, K. T.; Bhatia, S.; Mohamed, A. R. Post-combustion carbon dioxide capture: Evolution towards utilization of nanomaterials. *Renewable Sustainable Energy Rev.* **2012**, *16*, 2599−2609.

(8) Liu, L.; Nicholson, D.; Bhatia, S. K. Exceptionally high performance of charged carbon nanotube arrays for CO_2 separation from flue gas. *Carbon* **2017**, *125*, 245−257.

(9) D'Alessandro, D.; Smit, B.; Long, J. Carbon Dioxide Capture: Prospects for New Materials. *Angew. Chem., Int. Ed.* **2010**, *49*, 6058−6082.

(10) Jia, L.; Deng, R.; Song, H. Reversible removal of SO_2 at low temperature by Bacillus licheniformis immobilized on γ-Al_2O_3. *Bioresour. Technol.* **2011**, *102*, 524−528.

(11) Maurya, M.; Singh, J. K. A grand canonical Monte Carlo study of SO_2 capture using functionalized bilayer graphene nanoribbons. *J. Chem. Phys.* **2017**, *146*, 044704.

(12) Sitthikhankaew, R.; Predapitakkun, S.; Kiattikomol, R. W.; Pumhiran, S.; Assabumrungrat, S.; Laosiripojana, N. Comparative Study of Hydrogen Sulfide Adsorption by using Alkaline Impregnated Activated Carbons for Hot Fuel Gas Purification. *Energy Procedia* **2011**, *9*, 15−24.

(13) Lu, C.; Bai, H.; Su, F.; Chen, W.; Hwang, J. F.; Lee, H.-H. Adsorption of Carbon Dioxide from Gas Streams via Mesoporous Spherical-Silica Particles. *J. Air Waste Manage. Assoc.* **2010**, *60*, 489−496.

(14) Rahimi, M.; Singh, J. K.; Babu, D. J.; Schneider, J. J.; Muller-Plathe, F. Understanding Carbon Dioxide Adsorption in Carbon Nanotube Arrays: Molecular Simulation and Adsorption Measurements. *J. Phys. Chem. C* **2013**, *117*, 13492−13501.

(15) Rahimi, M.; Singh, J. K.; Muller-Plathe, F. CO_2 Adsorption on Charged Carbon Nanotube Arrays: A Possible Functional Material for Electric Swing Adsorption. *J. Phys. Chem. C* **2015**, *119*, 15232−15239.

(16) Drage, T. C.; Blackman, J. M.; Pevida, C.; Snape, C. E. Evaluation of Activated Carbon Adsorbents for CO_2 Capture in Gasification. *Energy Fuels* **2009**, *23*, 2790−2796.

DOI: 10.1021/acs.energyfuels.8b00649
Energy Fuels 2018, 32, 6090−6097

(17) Sircar, S.; Golden, T.; Rao, M. Activated carbon for gas separation and storage. *Carbon* **1996**, *34*, 1−12.
(18) Siriwardane, R. V.; Shen, M.-S.; Fisher, E. P.; Poston, J. A. Adsorption of CO_2 on Molecular Sieves and Activated Carbon. *Energy Fuels* **2001**, *15*, 279−284.
(19) Fang, H.; Kulkarni, A.; Kamakoti, P.; Awati, R.; Ravikovitch, P. I.; Sholl, D. S. Identification of High-CO_2-Capacity Cationic Zeolites by Accurate Computational Screening. *Chem. Mater.* **2016**, *28*, 3887−3896.
(20) Bonenfant, D.; Kharoune, M.; Niquette, P.; Mimeault, M.; Hausler, R. Advances in principal factors influencing carbon dioxide adsorption on zeolites. *Sci. Technol. Adv. Mater.* **2008**, *9*, 013007.
(21) Li, J.-R.; Ma, Y.; McCarthy, M. C.; Sculley, J.; Yu, J.; Jeong, H.-K.; Balbuena, P. B.; Zhou, H.-C. Carbon dioxide capture-related gas adsorption and separation in metal−organic frameworks. *Coord. Chem. Rev.* **2011**, *255*, 1791−1823.
(22) Sumida, K.; Rogow, D. L.; Mason, J. A.; McDonald, T. M.; Bloch, E. D.; Herm, Z. R.; Bae, T.-H.; Long, J. R. Carbon dioxide capture in metal−organic frameworks. *Chem. Rev.* **2012**, *112*, 724−781.
(23) Caskey, S. R.; Wong-Foy, A. G.; Matzger, A. J. Dramatic Tuning of Carbon Dioxide Uptake via Metal Substitution in a Coordination Polymer with Cylindrical Pores. *J. Am. Chem. Soc.* **2008**, *130*, 10870−10871.
(24) Di Biase, E.; Sarkisov, L. Molecular simulation of multi-component adsorption processes related to carbon capture in a high surface area, disordered activated carbon. *Carbon* **2015**, *94*, 27−40.
(25) Zhao, J.; Buldum, A.; Han, J.; Lu, J. P. Gas molecule adsorption in carbon nanotubes and nanotube bundles. *Nanotechnology* **2002**, *13*, 195.
(26) Suttisawat, Y.; Rangsunvigit, P.; Kitiyanan, B.; Williams, M.; Ndungu, P.; Lototskyy, M.; Nechaev, A.; Linkov, V.; Kulprathipanja, S. Investigation of hydrogen storage capacity of multi-walled carbon nanotubes deposited with Pd or V. *Int. J. Hydrogen Energy* **2009**, *34*, 6669−6675.
(27) Wang, W.; Peng, X.; Cao, D. Capture of Trace Sulfur Gases from Binary Mixtures by Single-Walled Carbon Nanotube Arrays: A Molecular Simulation Study. *Environ. Sci. Technol.* **2011**, *45*, 4832−4838.
(28) Ren, X.; Chen, C.; Nagatsu, M.; Wang, X. Carbon nanotubes as adsorbents in environmental pollution management: A review. *Chem. Eng. J.* **2011**, *170*, 395−410.
(29) O'Connell, M. *Carbon Nanotubes: Properties and Applications*; CRC Press: Boca Raton, FL, 2006.
(30) Cinke, M.; Li, J.; Bauschlicher, C.; Ricca, A.; Meyyappan, M. *Chem. Phys. Lett.* **2003**, *376*, 761−766.
(31) Liu, L.; Nicholson, D.; Bhatia, S. K. Impact of H_2O on CO_2 Separation from Natural Gas: Comparison of Carbon Nanotubes and Disordered Carbon. *J. Phys. Chem. C* **2015**, *119*, 407−419.
(32) Halder, P.; Maurya, M.; Jain, S. K.; Singh, J. K. Understanding adsorption of CO_2, N_2, CH_4 and their mixtures in functionalized carbon nanopipe arrays. *Phys. Chem. Chem. Phys.* **2016**, *18*, 14007−14016.
(33) Rahimi, M.; Babu, D. J.; Singh, J. K.; Yang, Y.-B.; Schneider, J. J.; Muller-Plathe, F. Double-walled carbon nanotube array for CO_2 and SO_2 adsorption. *J. Chem. Phys.* **2015**, *143*, 124701.
(34) Rahimi, M.; Singh, J. K.; Muller-Plathe, F. Adsorption and separation of binary and ternary mixtures of SO_2, CO_2 and N_2 by ordered carbon nanotube arrays: Grand-canonical Monte Carlo simulations. *Phys. Chem. Chem. Phys.* **2016**, *18*, 4112−4120.
(35) Aqel, A.; El-Nour, K. M. A.; Ammar, R. A.; Al-Warthan, A. Carbon nanotubes, science and technology part (I) structure, synthesis and characterisation. *Arabian J. Chem.* **2012**, *5*, 1−23.
(36) Babu, D. J.; Lange, M.; Cherkashinin, G.; Issanin, A.; Staudt, R.; Schneider, J. J. Gas adsorption studies of CO_2 and N_2 in spatially aligned double-walled carbon nanotube arrays. *Carbon* **2013**, *61*, 616−623.
(37) Nickmand, Z.; Aghamiri, S. F.; Talaie Khozanie, M. R.; Sabzyan, H. A Monte Carlo Simulation of the Adsorption of CO_2 and SO_2 Gases in Pure and Functionalized Single Walled Carbon Nanotubes. *Sep. Sci. Technol.* **2014**, *49*, 499−505.
(38) Yang, Y.-B.; Rahimi, M.; Singh, J. K.; Bohm, M. C.; Muller-Plathe, F. Adsorption and Condensation of SO_2 in Double-Walled Carbon Nanotube Arrays Studied by Monte Carlo Simulations and Simple Analytical Models. *J. Phys. Chem. C* **2016**, *120*, 7510−7521.
(39) Myers, A. L.; Prausnitz, J. M. Thermodynamics of mixed-gas adsorption. *AIChE J.* **1965**, *11*, 121−127.
(40) Cornell, W. D.; Cieplak, P.; Bayly, C. I.; Gould, I. R.; Merz, K. M.; Ferguson, D. M.; Spellmeyer, D. C.; Fox, T.; Caldwell, J. W.; Kollman, P. A. A Second Generation Force Field for the Simulation of Proteins, Nucleic Acids, and Organic Molecules. *J. Am. Chem. Soc.* **1995**, *117*, 5179−5197.
(41) Hummer, G.; Rasaiah, J. C.; Noworyta, J. P. Water conduction through the hydrophobic channel of a carbon nanotube. *Nature* **2001**, *414*, 188−190.
(42) Potoff, J. J.; Siepmann, J. I. Vapor−Liquid Equilibria of Mixtures Containing Alkanes, Carbon Dioxide, and Nitrogen. *AIChE J.* **2001**, *47*, 1676−1682.
(43) Ketko, M. H.; Kamath, G.; Potoff, J. J. Development of an Optimized Intermolecular Potential for Sulfur Dioxide. *J. Phys. Chem. B* **2011**, *115*, 4949−4954.
(44) Nath, S. K. Molecular Simulation of Vapor−Liquid Phase Equilibria of Hydrogen Sulfide and Its Mixtures with Alkanes. *J. Phys. Chem. B* **2003**, *107*, 9498−9504.
(45) Widom, B. Some Topics in the Theory of Fluids. *J. Chem. Phys.* **1963**, *39*, 2808−2812.
(46) Lorentz, H. A. *Ann. Phys.* **1881**, *248*, 127−136.
(47) Lemmon, E.; McLinden, M.; Friend, D. Thermophysical properties of fluid systems. In *NIST Chemistry WebBook, NIST Standard Reference Database Number 69*; Linstrom, P. J., Mallard, W. G., Eds.; National Institute of Standards and Technology (NIST): Gaithersburg, MD, 2005.
(48) Xu, X.; Song, C.; Wincek, R.; Andresen, J. M.; Miller, B. G.; Scaroni, A. W. Separation of CO_2 from power plant flue gas using a novel CO_2 molecular basket adsorbent. *Prepr. Pap.—Am. Chem. Soc., Div. Fuel Chem.* **2003**, *48*, 162−163.
(49) Do, D. D.; Do, H. D. Modeling of Adsorption on Nongraphitized Carbon Surface: GCMC Simulation Studies and Comparison with Experimental Data. *J. Phys. Chem. B* **2006**, *110*, 17531−17538.
(50) Mahdizadeh, S. J.; Tayyari, S. F. Influence of temperature, pressure, nanotube's diameter and intertube distance on methane adsorption in homogeneous armchair open-ended SWCNT triangular arrays. *Theor. Chem. Acc.* **2011**, *128*, 231−240.
(51) Myers, A. L.; Monson, P. A. Adsorption in Porous Materials at High Pressure: Theory and Experiment. *Langmuir* **2002**, *18*, 10261−10273.
(52) LeVan, M. D.; Vermeulen, T. Binary Langmuir and Freundlich isotherms for ideal adsorbed solutions. *J. Phys. Chem.* **1981**, *85*, 3247−3250.
(53) Do, D. D. *Adsorption Analysis: Equilibria and Kinetics*; Imperial College Press: London, U.K., 1998.
(54) Agnihotri, S.; Mota, J. P.; Rostam-Abadi, M.; Rood, M. J. Adsorption site analysis of impurity embedded single-walled carbon nanotube bundles. *Carbon* **2006**, *44*, 2376−2383.
(55) Bienfait, M.; Zeppenfeld, P.; Dupont-Pavlovsky, N.; Muris, M.; Johnson, M. R.; Wilson, T.; DePies, M.; Vilches, O. E. Thermodynamics and structure of hydrogen, methane, argon, oxygen, and carbon dioxide adsorbed on single-wall carbon nanotube bundles. *Phys. Rev. B: Condens. Matter Mater. Phys.* **2004**, *70*, 035410.

DOI: 10.1021/acs.energyfuels.8b00649
Energy Fuels 2018, 32, 6090−6097